Acta Astronautica 210 (2023) 212–223

Contents lists available at ScienceDirect

Acta Astronautica

journal homepage: www.elsevier.com/locate/actaastro

Research paper

The "Effect of Marangoni Convection on Heat Transfer in Phase Change Materials" experiment

J. Porter [a], A. Laverón-Simavilla [a], M.M. Bou-Ali [b], X. Ruiz [c], F. Gavalda [c], J.M. Ezquerro [a], P. Salgado Sánchez [a,*], U. Martínez [a], D. Gligor [a], I. Tinao [a], J. Gómez [a], J. Fernández [a], J. Rodríguez [a], A. Borshchak Kachalov [a], V. Lapuerta [a], B. Seta [d], J. Massons [c], D. Dubert [c], A. Sanjuan [b], V. Shevtsova [b,e], L. García-Fernández [f]

[a] E-USOC, Center for Computational Simulation, Escuela Técnica Superior de Ingeniería Aeronáutica y del Espacio, Universidad Politécnica de Madrid, Spain
[b] Mechanical and Manufacturing Department, Mondragon University, Mondragon, Spain
[c] Facultat de Química, Universitat Rovira i Virgili, Tarragona, Spain
[d] Department of Mechanical Engineering, Technical University of Denmark, Kongens Lyngby, Denmark
[e] IKERBASQUE, Basque Foundation for Science, Bilbao, Spain
[f] Departamento de Estructura de la Materia, Física Térmica y Electrónica, Facultad de Ciencias Físicas, Universidad Complutense de Madrid, Spain

ARTICLE INFO

Keywords:
Microgravity
Phase change materials
Thermocapillary effect
Thermal control

ABSTRACT

Present as well as future challenges of space exploration point to the need for improved thermal control systems. The "Effect of Marangoni Convection on Heat Transfer in Phase Change Materials" experiment, which is approved by ESA for execution on board the International Space Station, aims to contribute directly to current knowledge and basic understanding of heat and mass transport in phase change materials (PCMs) that incorporate a free surface in reduced gravity. The experiment will apply fixed temperatures to opposite ends of PCM samples held in cuboidal and cylindrical containers in order to drive controlled melting and solidification cycles that will be observed by means of optical cameras. The recorded images will be complemented by thermal measurements at key positions along the samples, which will allow different thermocapillary flow regimes to be distinguished according to their temporal dynamics. It is anticipated that thermal Marangoni (thermocapillary) convection will increase the heat transfer rate in these PCM devices by a significant factor (on the order of two or more) compared to melting governed by thermal diffusion (conduction). If the PCM designs prove robust, the experiment results can be expected to lead to substantial improvements in future designs for passive PCM applications in space missions.

1. Introduction

There is widespread and accelerating interest in energy storage systems that can reduce waste and improve efficiency, motivated in part by the urgent need to combat climate change and limit environmental degradation. Phase change materials (PCMs), which are characterized by their ability to store and release large amounts of thermal energy over a determined temperature range, are an attractive way to control temperature and reduce energy loss in a range of applications including air conditioning [1,2], electronics [3], manufacturing [4,5], and the clean energy industry [6,7].

The energy storage potential of typical PCMs depends primarily on their heat of fusion, which determines the thermal energy captured during melting and released during solidification. To be most effective, this heat of fusion should be as large as possible given the material constraints and the need for an appropriate melting temperature T_M. The incorporation of a PCM device increases the thermal inertia of the system and helps maintain its temperature near T_M. A wide assortment of systems, both passive and active, can be made more efficient by including suitable PCM devices.

Nowadays, the practical choices for PCMs cover a wide range of operating temperatures and include both natural and synthetic materials [8,9]. Inorganic PCMs, typified by hydrated salts, have high latent heats of fusion and high thermal conductivities but can be corrosive in contact with metals and other materials, and may suffer from irregular melting (phase separation) and the problem of super cooling. Organic PCMs, typified by alkanes and fatty acids, are non-reactive and stable, with more regular melting and freezing cycles, but

* Corresponding author.
E-mail address: pablo.salgado@upm.es (P. Salgado Sánchez).

https://doi.org/10.1016/j.actaastro.2023.05.026
Received 25 December 2022; Received in revised form 14 April 2023; Accepted 15 May 2023
Available online 19 May 2023

are hampered in many applications by low thermal conductivity, which reduces responsiveness and requires long charge and discharge cycles.

Various strategies for improving the performance of organic PCMs by augmenting their heat transport capacity have been proposed. Active systems may incorporate coolant loops and pumps, for example, as in the NASA Phase Change HX Project [10]. Higher heat transfer rates can be achieved in passive systems simply by placing the PCM in contact with more conductive materials (see, e.g., Refs. [11–14]) or by increasing the effective thermal diffusivity of the PCM through the addition of dispersed nanoparticles (see, e.g., Refs. [15,16]) to create Nano-enhanced Phase Change Materials (NePCMs). Note that these strategies involve the incorporation of additional materials that, with the exception of nanoparticles, will require a notable increase in the mass and volume of the thermal control device to maintain the same energy storage capacity.

In many situations, the limitations of low conductivity can be alleviated in part by natural convection in the liquid, which enhances the total heat transfer rate of the system. Since the seminal work of Gau and Viskanta [17], a number of different theoretical, numerical and experimental investigations have been undertaken to determine the role of convection in the melting of PCMs (see, e.g., Refs. [18–21]). The recent review of Dhaidan and Khodadadi [22] looked at the influence of the main governing parameters including Stefan and Rayleigh numbers, which characterize the effect of the PCM latent heat and the relative importance of convection and conduction, respectively. The influence of container geometry was also considered, from rectangular cavities to spherical capsules and tubes.

A special area of application for PCM devices is space exploration, where PCMs have a long history of use. Nearly every space mission must deal with significant fluctuations in temperature, so designing an efficient and effective thermal control system is a critical requirement — even more so in the case of manned missions. PCM devices, with their potential for simple passive temperature control, can be expected to play an important role in future space exploration. The use of PCM devices in space missions also raises particular concerns that have discouraged their wider use. For one thing, the increase of mass and volume that accompanies most heat transport enhancement strategies is something to be avoided as much as possible. Furthermore, the microgravity environment of orbiting satellites or the International Space Station (ISS) precludes the use of natural (buoyant) convection as an additional heat transport mechanism. The high pressures that can result from the volume changes associated with melting and solidification can lead to stress damage and the inconvenient formation of bubbles (voids) during melting. If organic PCMs, with their notable advantages, are to be used in passive configurations in reduced gravity conditions, it is important to find simple, robust, and effective solutions to their main drawbacks. One idea is to take advantage of the fact that, if the PCM design incorporates a free surface, the temperature gradient inherent to its operation induces variations in surface tension that drive thermocapillary convection. Furthermore, the presence of the gas layer helps alleviate the problem of disruptive pressure changes (and related bubbles/voids) associated with the thermal expansion of the material during phase change.

In this manuscript, we introduce the "Effect of Marangoni Convection on Heat Transfer in Phase Change Materials" (MarPCM) project, which combines theoretical and experimental investigations into the potential of thermocapillary (Marangoni) convection to expedite melting of organic PCMs and make more efficient use of their energy storage capacity. The project is approved by ESA for implementation on the ISS and is backed by the Spanish Delegation of the CDTI and funded by the Ministerio de Ciencia e Innovación under Projects No. PID2020-115086GB-C31, PID2020-115086GB-C32 and PID2020-115086GB-C33.

The MarPCM experiment aims to definitively test heat enhancement strategies based on the thermocapillary effect during complete melting and solidification cycles, something that is only possible in the sustained microgravity environment of the ISS. The scientific consortium encompasses four research groups from leading Spanish universities in microgravity research: the 'Fluid Mechanics' research group from Mondragon University (MU), the 'Digital Processing of Signals in Aerospace and Biomedics' (SPABE) group from Universitat Rovira i Virgili (URV), and the 'Aerospace Science and Technology' research group from the Technical University of Madrid (UPM), which is coordinating the project. The MU team has extensive experience in the design and development of new experimental procedures and in the experimental characterization of thermophysical and transport properties in liquid systems. The URV team has extensive expertise in modeling complex fluid systems and have also worked intensively on the characterization of microgravity environments through the use of digital signal processing techniques, supporting various experiments on the ISS. The UPM team has extensive experience in conducting microgravity experiments on board the ISS, as host of the Spanish User Support and Operations Centre (E-USOC), and a successful research program investigating fluid dynamical phenomena including PCMs with natural and thermocapillary convection, interfacial instabilities, liquid bridges, and the effects of applied vibrations.

The manuscript is structured as follows. In Section 2, we provide a review of the most relevant results regarding PCM melting in microgravity and the scientific motivation of the project. In Sections 3 and 5, we describe the objectives of the MarPCM project and its expected results, respectively. A description of the experiment and some preliminary ground experiment results are provided in Sections 4 and 6, with final conclusions offered in Section 7.

2. Scientific motivation and background

As noted above, nearly every space mission must deal with significant fluctuations in temperature. These may be caused, for example, by the cyclic variation of radiation fluxes or the heat generated by electrical and propulsion systems. Small satellites, which are especially relevant nowadays, have particularly low thermal inertia and may suffer under extreme temperature changes. Designing an efficient and effective thermal control system is thus a critical requirement. PCM devices, with their potential for simple and passive temperature control, have a long history of applications in space missions [23] – going back to the Apollo 15 Lunar Rover Vehicle, Skylab SL-1, and the Venera 8–10 missions – and can be expected to play an important role in future space exploration as well. For instance, in the context of the ESA Moon Village programme [24], more effective designs could help maintain habitable conditions [25] despite the extreme temperature difference between the lunar day and night.

However, some of the difficulties mentioned earlier have discouraged wider use. These problems include low heat transfer rates, high pressures (leading to stress damage) resulting from volume changes and the inconvenient formation of bubbles (voids) during melting. Except for the use of dispersed nanoparticles, most of the passive solutions that have been considered for improving heat transfer through the addition of conducting material bring with them the disadvantage of increased mass and/or size of the PCM device. Furthermore, by themselves, they do nothing to restore the convective motion that can significantly improve heat transfer properties on ground. If organic PCMs are to be used in passive configurations in reduced gravity conditions, it is important to find simple, robust, and effective solutions to their main drawbacks.

In microgravity, the thermocapillary effect, which also induces convective flow, can act as an alternative heat transport mechanism to that of natural convection. The recent numerical work of Refs. [27,28] was the first to point out the positive effect of thermocapillary flow during the melting of PCMs. In Ref. [27], the authors analyzed the melting process in a semi-circular geometry in microgravity. Depending on the applied temperature, enhancement of heat transport by a factor of up to 5.2 was observed compared to the purely conductive case. In

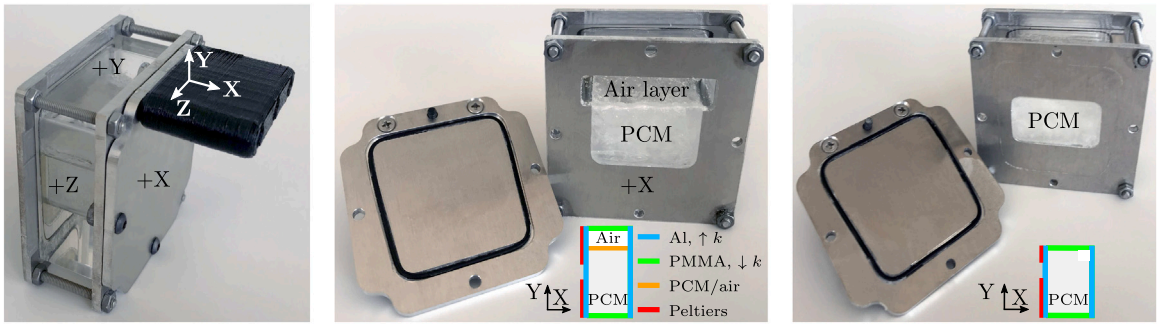

(a) General view (b) *Marangoni cell* (c) *Reference cell*

Fig. 1. Photos of the Marangoni and reference cells of the TEPiM experiment. The sketches in panels (b, c) show the elements of the cell most relevant for the melting process. *Source:* Reproduced from Ref. [26]

Ref. [28], an analogous process in square geometry was investigated under the combined effect of thermocapillary and buoyant convection. Numerical simulations showed, for higher applied temperatures, heat transport enhancement by a factor of up to 1.38.

In general, flows driven by the thermocapillary effect have attracted sustained interest from the scientific community due to their relevance in a range of technological processes such as crystal growth [29–32], combustion [33], welding [34], and in other phenomena like the migration of bubbles, the spreading of drops or the motion of dispersed solid particles in fluid layers [35]. In the context of crystal growth, in particular, a series of investigations uncovered the mechanisms for convective instability in rectangular geometry [29,36,37] and described the associated flow regimes in single-phase (liquid) systems, which are governed mainly by the Prandtl number and the container aspect ratio [38,39]. Analogous flow regimes are expected to be relevant in the context of PCMs [31,32], as discussed below.

The numerical predictions of Refs. [27,28] were experimentally confirmed by the "Thermocapillary Effects in Phase change materials in Microgravity" (TEPiM) experiment [26,40,41]. Motivated by these results, a series of investigations have analyzed PCM melting with thermocapillary effects and the main findings of these are summarized here.

2.1. The "Thermocapillary Effects in Phase change materials in Microgravity" experiment

The TEPiM experiment investigated the melting dynamics and heat transfer characteristics of the alkane n-octadecane in the presence of thermocapillary convection in microgravity, with the principal objective of quantifying the contribution of thermocapillary flow to the heat transfer rate [26]. The experiment was conducted on parabolic flights [42], which provided repeated periods of microgravity lasting (approximately) 20 s, as part of the ESA educational program "Fly Your Thesis! 2016" during the 65th ESA Parabolic Flight campaign.

The core set-up of the experiment consisted of three pairs of cuboidal cells of width $W = 35$ mm, length $L = 20$ mm, and increasing heights $H = 20$, 25 and 30 mm. Each pair included a Marangoni (thermocapillary) cell, which incorporated a 5 mm thick layer of air above the PCM in order to support thermocapillary convection, and a reference cell containing only the PCM, wherein melting was dominated by thermal conduction (diffusion). Both types of cells were subjected to controlled thermal conditions, allowing for a direct comparison of the phase change in each scenario [26,40]. Some photos of the experiment cells are shown in Fig. 1.

For the geometry selected in the experiments, the timescale of thermal diffusion is on the order of minutes: $\tau_k = L^2/\alpha \sim \mathcal{O}(10^3)$ s [40], while that associated with convective transport driven by the thermocapillary effect is on the order of tens of seconds: $\tau_k\, \Gamma^2/\mathrm{Pr} \sim \mathcal{O}(10)$ s [43]. Here, $\alpha = k_L/(\rho_L\, c_{pL}) \simeq 8.6 \times 10^{-8}$ m^2/s is the thermal diffusivity and $\mathrm{Pr} \simeq 52.7$ is the Prandtl number of liquid n-octadecane, with $\Gamma = H/L \sim \mathcal{O}(1)$. Because of this, each experiment was performed in two stages. During the first (preparation) stage, which lasted several minutes, the PCM was subjected to temperatures of 0 °C and 80 °C, respectively, along the upper and lower portions of one of its lateral boundaries. This initial stage, with conduction-driven melting near the lower, heated portion of the wall, began approximately 8 min before the relevant microgravity period and produced a drop-like region of liquid PCM surrounded by solid, which prevented the liquid PCM from making contact with the air.

About 40 s prior to the microgravity period, the temperature along the lateral boundary was made approximately uniform at 80 °C. The subsequent (rapid) melting of the solid along the upper portion of the wall produced a controlled liquid/air interface at the beginning of the microgravity period so that the development of thermocapillary convection could be concentrated during the available 20 s of reduced gravity and separated as much as possible from the effects of buoyancy. As the solid PCM separating the liquid and the air layer melted, the liquid/air interface was created; see the left panel of Fig. 2(a). The resulting thermocapillary convection increased the heat transfer rate and locally accelerated the melting process, as reflected in the rapid advance of the solid/liquid (S/L) front near the liquid/air interface; see the left panel of Fig. 2(b). During the periods of reduced gravity, the dynamics of the free surface were controlled by pinning the contact line to preserve a (nearly) flat interface [26,40]. More details can be found in Refs. [26,40], which describe the full experimental sequence including the time dependence of the cell temperatures and gravity.

The melting process was monitored with two cameras, which provided lateral and overhead images of the developing phase change, six thermocouples, which measured the temperature at relevant locations, and the airplane accelerometers. The melting process was evaluated based on the evolution of the S/L front and the associated (cross-sectional) liquid area A. Fig. 2(c) shows the evolution of A in microgravity. The results from thermocapillary (solid markers) and reference experiments (open markers) are compared, for each value of $H = 20$, 25, 30 mm, after subtracting the initial area at the beginning of microgravity and measuring time relative to that point.

During reduced gravity, A increased in a nearly linear fashion, consistent with the fact that the microgravity time of 20 s was much shorter than the timescale of the phase change, and the data from the different experiments collapse to the same line. The enhancement factor $\mathcal{G}$ can be expressed by comparing the melting rates between thermocapillary and reference experiments,

$$\mathcal{G} = \frac{A_{\mathrm{Ma}}}{A_{\mathrm{ref}}}, \tag{1}$$

which are proportional to the inverse of the characteristic time in each case. Recall that, in reference experiments, the melting rate was principally due to conductive heat transport while, in Marangoni experiments, it reflected the contribution of thermocapillary convection.

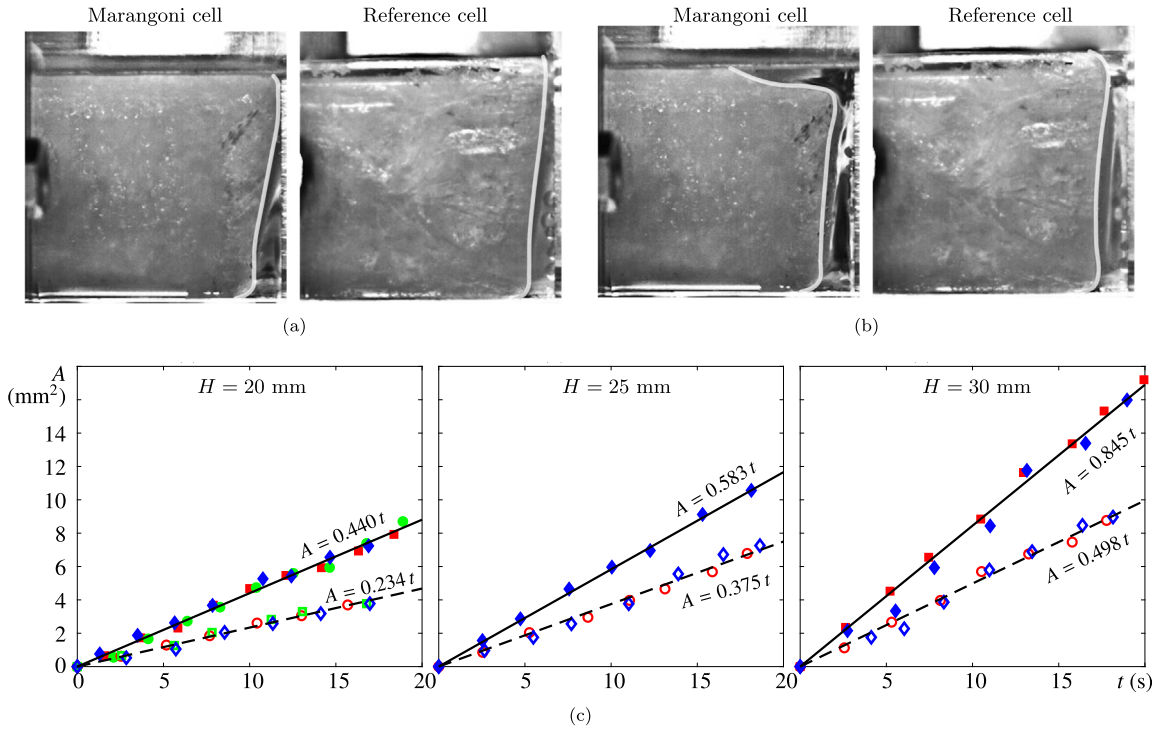

Fig. 2. (a, b) Snapshots showing the evolution of thermocapillary (left) and reference (right panels) experiments just before (a) and after (b) the microgravity period; the location of the solid/liquid interface at the lateral wall is highlighted. (c) Melting in microgravity for thermocapillary (solid) and reference experiments (open markers) with different PCM heights H. Detail of the liquid area evolution (in mm^2) during microgravity.
Source: Adapted from Ref. [41]

The influence of the cell geometry was apparent in these experiments, as can be seen by comparing the different panels of Fig. 2(c). The experimental measurements for each value of H, later extended by a series of numerical simulations in Ref. [41], clearly demonstrate that $\mathcal{G}$ increases with the (cross-sectional) aspect ratio $\Gamma = L/H$. This can be explained by the fact the thermocapillary convection develops within a relatively localized layer near the free surface; see the left panel of Fig. 2(b). As long as this layer is thinner than H, the contribution of thermocapillary convection is localized and remains comparable, while that of conduction increases with H. Note that the values of Γ explored in TEPiM were all of order unity, covering a range where the layer dominated by thermocapillary convection neither interacts with the bottom of the container nor is negligible as it would be in the limit of $\Gamma \to 0$. The results suggest that the greatest relative enhancement would be achieved when H is comparable to the (average) thickness of the thermocapillary layer.

Overall, the TEPiM experiment demonstrated the potential of the thermocapillary effect to enhance heat transport in microgravity, and suggested it could be a viable alternative for designing more efficient thermal control systems based on PCMs in future space missions. A detailed description of the experiment set-up and associated results can be found in Ref. [26] and Refs. [40,41], respectively.

2.2. Recent results on PCM melting with thermocapillary effects

The promising results of the TEPiM experiment motivated further research, including the detailed numerical analysis of thermocapillary flows during the melting of n-octadecane in rectangular containers in microgravity presented in Refs. [44,45]; these results considered an adiabatic thermocapillary interface, i.e., with zero Biot number (Bi). The effects of thermocapillary flows were shown to depend crucially on Γ and the Marangoni number

$$\mathrm{Ma} = \frac{\gamma L \Delta T}{\mu \alpha}, \tag{2}$$

which quantifies the relative importance of the convective heat transport driven by thermocapillary flow and that driven by thermal conduction. Here, γ refers to the thermocapillary coefficient, ΔT is the applied temperature difference and μ is the liquid dynamic viscosity. The simulations in those works covered a wide range of $\mathrm{Ma} \in (6000, 300000)$ and $\Gamma \in [1.5, 23)$.

In small Γ containers, the thermocapillary flow is initially characterized by a flow structure of co-rotating vortices located in a thin liquid layer near the thermocapillary interface that, as the melting progresses, slowly evolves into a steady vortical structure with a size comparable to the container dimensions.

As Ma is raised, a complex oscillatory mode appears, characterized by pulsation of the flow structure; this mode is analogous to the one described by Peltier and Biringen [37] in liquid rectangular domains and referred to as an *oscillatory standing wave* (OSW). The melting process for $\Gamma = 2.25$ and a large applied Ma is illustrated in Fig. 3(a), which shows the evolution of the S/L front and the temperature field. The qualitative similarity between the predicted S/L front at $\tau = 0.0512$ and the experiments shown in the left panel of Fig. 2(b) is evident.

In large Γ containers, the thermocapillary flow initially adopts a structure with a large vortex spanning the liquid domain. With increasing Ma, this structure splits into a series of smaller vortices to create a *steady multi-cellular* structure [47]. With further increase, the flow undergoes a transition to a *hydrothermal traveling wave* (HTW) characterized by the periodic creation of vortices near the cold boundary (i.e., either the cold wall or the S/L front) that travel inward [36].

The melting process for $\Gamma = 12$ and a large applied Ma is shown in Fig. 3(b), illustrating the evolution of the S/L front and the temperature field typical of HTWs. Finally, in containers of intermediate Γ, the flow displays a series of transitions as Ma is increased: from steady flow to HTWs, back to steady flow, and then to the OSW mode.

These flow regimes are summarized in terms of Ma and Γ in Fig. 4(a), with simulations denoted by markers and color-coded according to the observed mode: steady (black), OSW (blue), HTW (red). The

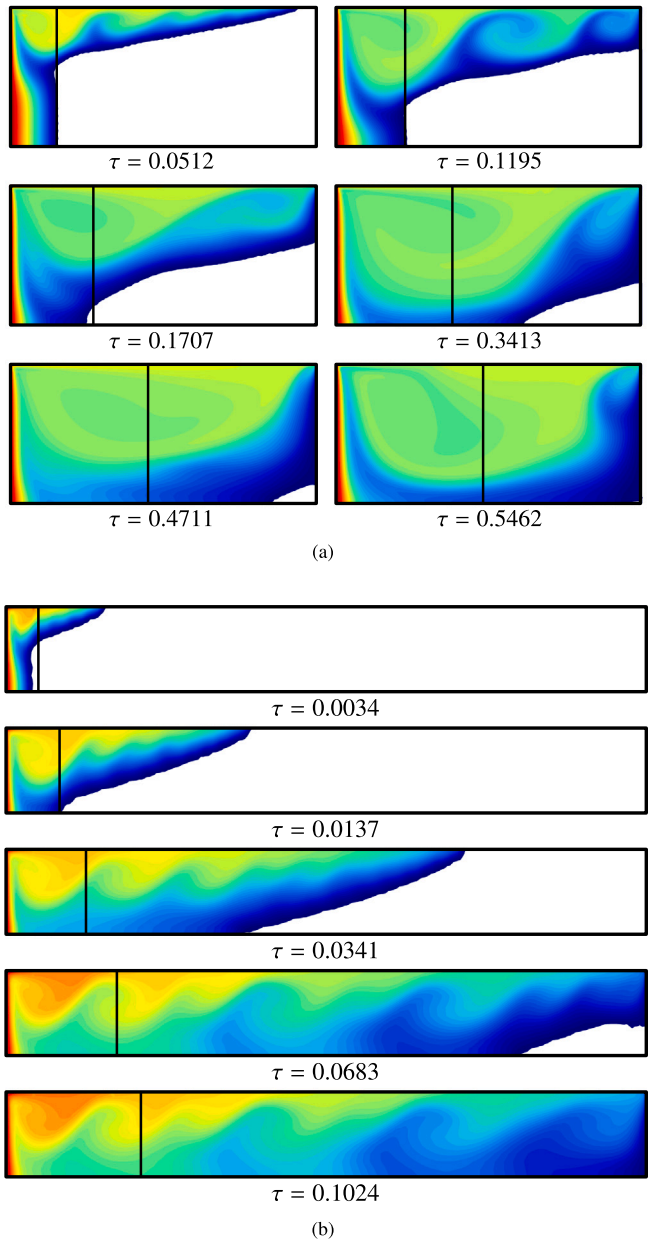

Fig. 3. PCM melting in rectangular geometry with Ma = 186224 and Bi = 0 for (a) Γ = 2.25 and (b) Γ = 12, where the thermocapillary flow is characterized by the appearance of OSW and HTW modes, respectively. The black vertical lines indicate where the position of the S/L interface would be with purely diffusive heat transport. The color map shows the temperature field.
Source: Adapted from Ref. [44]

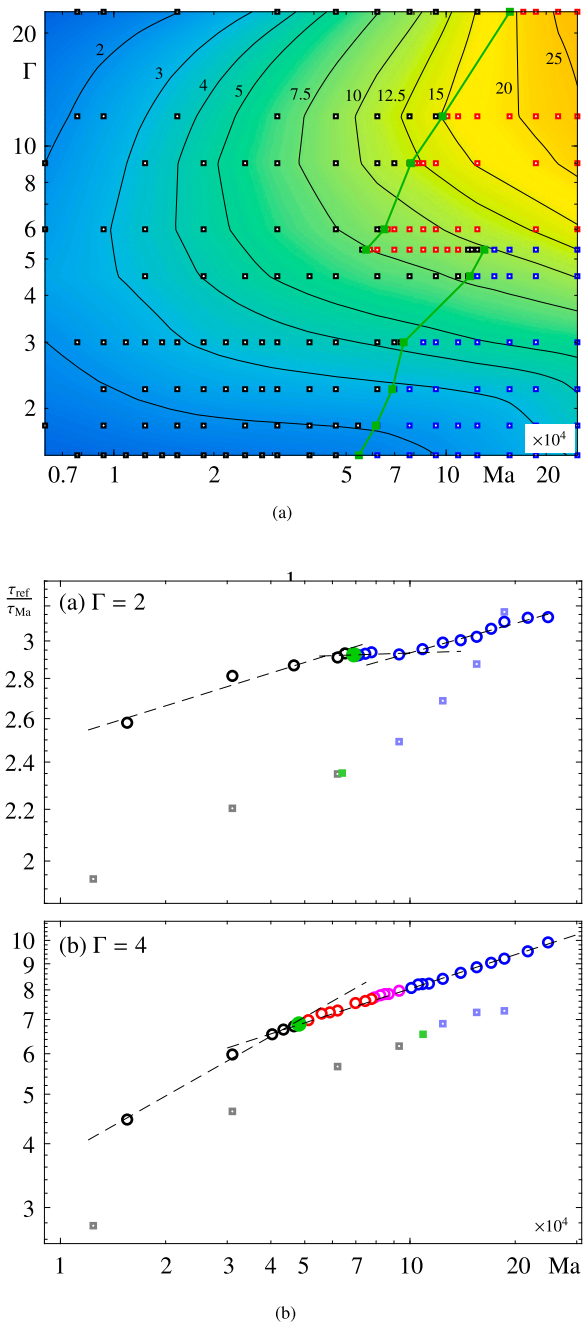

Fig. 4. (a) Contours showing the enhancement ratio $\mathcal{G}$ in rectangular geometry as a function of Ma and Γ and the instability map indicating the type of thermocapillary flow observed during melting: steady (black), HTW (red), OSW (blue), onset (green). (b) Enhancement ratio in cylindrical geometry as a function of Ma for (a) $\Gamma = 2$ and (b) $\Gamma = 4$. Simulations are indicated with circular markers and are color-coded accordingly the type of thermocapillary flow observed: steady (black), HTW (red), transition from HTW to OSW (pink) and OSW (blue). The onset of oscillatory convection is highlighted in green. Results in rectangular geometry (square markers) are included for comparison. (For interpretation of the references to color in this figure legend, the reader is referred to the web version of this article.)
Source: Reproduced from Refs. [44,46]

critical boundary for oscillatory flow is marked by a solid green line. The enhancement factor $\mathcal{G}$, defined here as the ratio between melting times τ in simulations with purely conductive transport (denoted by the subscript 'ref') and with the thermocapillary effect (denoted by 'Ma'),

$$\mathcal{G} = \frac{\tau_{\mathrm{ref}}}{\tau_{\mathrm{Ma}}}, \tag{3}$$

is shown using a contour map. This factor $\mathcal{G}$ ranges from approximately 2 to 25. For fixed Γ, it increases with Ma, reflecting the growing importance of the thermocapillary flow. For fixed Ma, on the other hand, there exists an optimal Γ that maximizes $\mathcal{G}$ [44]. Recently, Ref. [48] extended this analysis and considered other PCMs with moderate T_M, including n-nonadecane and n-eicosane from the family of alkanes, and gallium.

As can be observed in Fig. 3(a), the thermocapillary-driven phase change is often accompanied by a final stage dominated by conduction where the solid PCM near the cold boundary slowly melts. This phase lasts a certain percentage of the total melting time and sets a lower bound on τ_{Ma}. In the recent work of Ref. [49], the use of trapezoidal and triangular containers was proposed to optimize the melting process. By

inclining the cold lateral wall, in particular, melting can be accelerated substantially with respect to the rectangular case, with an optimal reduction of τ_{Ma} by a factor of 3 in the limiting case of a right triangle.

The basic results in rectangular geometry were also extended to include the effect of heat exchange across the thermocapillary interface. In Ref. [50], the authors explored pattern selection and heat transfer characteristics during melting in small Γ containers in contact with an air layer whose temperature was assumed to match the applied temperatures at the lateral walls and to vary linearly between them. The effect of Ma and Bi, which characterizes the heat exchanged across the PCM/air interface, was analyzed. Several different flow regimes were distinguished, including the OSW and HTW modes, a novel type of *thermal traveling wave*, and transitions where the oscillatory flow undergoes a homoclinic bifurcation. The effect of Bi on heat transport was also investigated and shown to be particularly relevant for small Ma.

The variety of flow transitions mentioned above were explained using the concept of an effective aspect ratio Γ_{eff} and Marangoni number Ma_{eff} in the liquid phase, which is bounded by the slowly advancing S/L front and, thus, has a dynamic boundary condition. The strategy of characterizing this by dynamic dimensionless parameters was explored in Ref. [39] and used to compare the flow transitions in rectangular domains of pure liquid with those observed during melting. The temporal evolution of the phase change was characterized by Γ_{eff} and Ma_{eff} and very good agreement was found with the dynamics observed in the equivalent rectangular containers of pure liquid over the explored range of parameters. Note that regardless of the value of Γ, the initial $\Gamma_{\text{eff}} \to 0$. In shallow containers, Γ_{eff} rapidly increases and, therefore, the HTW mode is consistently selected. In deep containers, Γ_{eff} is more limited and a preference for the OSW mode at high applied Ma is observed.

The results obtained with rectangular containers were extended to cylindrical (liquid bridge) geometry in a series of investigations. In Ref. [46], a detailed numerical exploration of the axisymmetric melting of PCMs with a liquid bridge geometry in microgravity was presented. Both steady and oscillatory flow regimes were found for small and large Ma, respectively, with their properties depending on $\Gamma = L/R$ — defined here by the liquid bridge length L and its radius R — and characterized by the appearance of either OSWs or HTWs. The contribution of the thermocapillary effect to the overall heat transfer rate during the phase change was analyzed over a wide range of Ma. In Fig. 4(b), the enhancement factor is shown for $\Gamma = 2, 4$, with markers denoting simulations and color-coded according to the observed mode: steady (black), OSW (blue), HTW (red) and transition from HTW to OSW (pink); the critical boundary for oscillatory flow is marked in green. Compared to rectangular geometry, for which the enhancement factor is shown for comparison with lighter rectangular markers, an additional improvement of approximately 50% is achieved with the liquid bridge set-up. This improved performance is related to the larger free-surface-area-to-PCM-volume ratio of liquid bridges.

In Ref. [51], the complete three-dimensional problem, which was given the name *melting bridge*, was analyzed numerically for the first time. The analysis was conducted for moderate-to-large applied ΔT and the melting dynamics were characterized in terms of frequency and the wave patterns in longitudinal and azimuthal directions. Again, standing waves, traveling waves and transitions between different modes were observed. In Ref. [52], these transitions were analyzed for a melting bridge of aspect ratio unity and compared to those observed in cylindrical liquid bridges (no solid phase) of $\Gamma = 0.7, 1$.

Finally, these microgravity results were extended to include the combined effects of natural and thermocapillary convection in both rectangular [53] and liquid bridge [54] geometries. In general, the presence of normal vertical gravity was shown to stabilize the dynamics of the flow in rectangular containers, delaying the appearance of oscillatory convection. Regarding heat transport, the results were qualitatively similar to those obtained in microgravity with the exception of short containers, where the presence of thermocapillary flows was found to retard the melting process compared to that driven solely by natural convection. In liquid bridge geometries, on the other hand, the influence of axial gravity on the heat transfer rate depends on whether the thermocapillary flow is opposed by the buoyant force, as when the PCM is heated from above, or acts in the same sense, as when it is heated from below; the heat transfer rate is reduced in the first case and increased in the second.

The various results summarized above highlight both the interesting mass and heat transport characteristics that can be observed in PCM systems that incorporate a free surface and the effectiveness of thermocapillary flows to expedite melting. The aim of the MarPCM project is to extend the level of scientific understanding in this area and perform a series of controlled experiments in microgravity to evaluate the performance of thermocapillary-enhanced PCM devices. The specific objectives are described below.

3. Project objectives

The principal objective of the MarPCM project is to provide the necessary theoretical and experimental work needed to evaluate the effectiveness of thermocapillary convection and related strategies, like nanoparticles [55,56], for improving PCM devices and to support the development of the microgravity experiment planned for the ISS.

The general objectives of the MarPCM project are as follows.

1. *Quantify the effect of thermal Marangoni convection on the heat transfer rate (melting and solidification times) in comparison with the case of pure thermal diffusion (conduction)*.
   This will be accomplished by comparing heat transfer in a cuboidal cell with a PCM/air interface and Marangoni convection with that in a closed cuboidal cell holding a PCM of equal dimensions but no free interface and subjected to the same applied temperatures.
2. *Compare the effectiveness of thermal Marangoni convection for a PCM with a cuboidal geometry (possessing one rectangular free surface) and for cylindrical geometry (a liquid bridge configuration when melted)*.
   This will be based on the difference in heat transfer rate between a cuboidal cell and a cylindrical cell with the same PCM material and subjected to the same applied temperatures. For comparable dimensions (length, aspect ratio), the cylindrical cell will have a greater surface area and is expected to be more affected by thermocapillary convection.
3. *Determine the dependence on temperature gradient (applied temperature difference) of the contribution from thermal Marangoni convection, including the dependence on dynamical regimes*.
   Since the Marangoni number is proportional to the temperature difference, this is a key parameter in determining the strength and type of thermocapillary convection (i.e., steady or oscillatory). Its influence on heat transfer will be investigated in each experiment cell by applying different temperatures over a series of runs selected to cover each of the principal regimes, in particular, capturing the transition from steady to oscillatory convection. The transition to oscillatory (and other types of) dynamics will be determined from the time dependence of the temperature field measured at selected points. The relationship between the spatial structure of the supercritical (oscillatory) flow and the geometry/morphology of the liquid domain will be analyzed as well.
4. *Evaluate the robustness of the proposed design and any practical difficulties associated with maintaining a free surface, and PCM performance in general, over a series of melting and freezing cycles*.
   This evaluation will be made based on the overall performance of the cell designs and will be an important factor in comparing the cuboidal and cylindrical geometries.

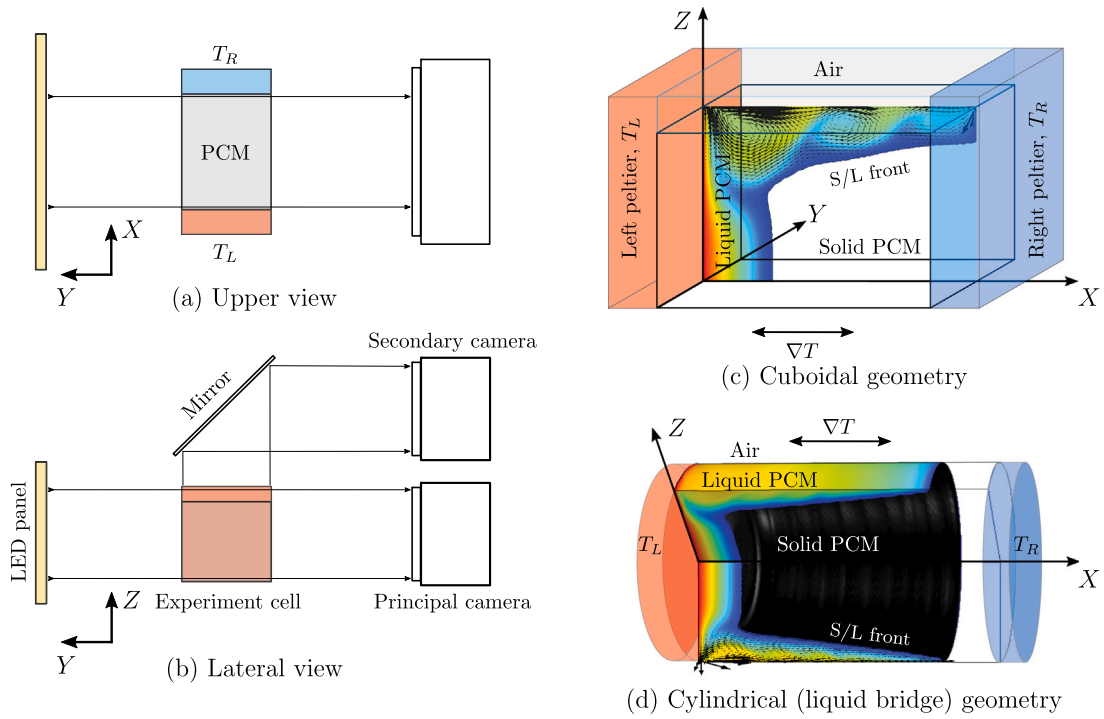

Fig. 5. (a, b) Schematic diagram of the experiment set-up showing (a) upper and (b) lateral views. (c, d) Isometric sketches of the cells for (c) cuboidal and (d) cylindrical (liquid bridge) geometries.

5. *Compare the heat transport efficiency of a pure PCM with a NePCM (containing metallic nanoparticles).*
   This will be done by comparing the performance of the pure PCM in the cuboidal cell (referred to above) with that of the NePCM in an identical cuboidal cell.
6. *Investigate the effect of mechanical vibrations with and without thermal Marangoni convection.*
   This evaluation will be done using real accelerometric signals.

4. The experiment

Fixed temperatures will be applied to opposite ends of the PCM in order to establish a controlled melting or solidification process, which will be observed by means of optical cameras and appropriate illumination. Sketches illustrating the upper and lateral views of the set-up are shown in Fig. 5(a, b).

The PCM samples will be held in containers constructed with two different geometries: cuboidal and cylindrical, as illustrated in panels (c, d) of Fig. 5. Each of these containers (called Marangoni cells) will be designed to passively maintain the PCM/gas interface by pinning the contact line to a sharp edge of the container so that the interface between the liquid PCM and the air (gas) is well controlled during melting and solidification. One of the cuboidal cells will be completely filled with the PCM and used as a reference (called the Reference cell) where Marangoni convection is absent. This Reference cell will provide measurements of PCM heat transfer driven purely by conduction to be compared with that in the Marangoni cell experiments.

The cuboidal cells will contain a volume of PCM of approximately $22.5 \times 15 \times 26.5$ mm^3 (length × height × depth), with a cross-sectional aspect ratio $\Gamma = L/H = 1.5$, and a volume of air (gas) of approximately $5 \times 22.5 \times 26.5$ mm^3, if applicable. In the Marangoni cells, the volume variation due to the phase change will be naturally accommodated by the air layer, while in the Reference cell, this will be taken into account as part of the cell design and compensated for.

The cylindrical cells, on the other hand, will contain PCM volumes of approximately 2848π and 712π mm^3 (i.e., radii of 11.25 and 5.625 mm and a length of 22.5 mm) corresponding to aspect ratios $\Gamma = L/R = 2, 4$, and will be surrounded by a layer of air that is approximately 5 mm wide. Note that the cuboidal cell width of 26.5 mm is selected to provide a total PCM volume approximately equal to that of the cylindrical cell with $\Gamma = 2$, which allows for a direct comparison of the phase change with equal volume but different free surface-to-volume ratios.

The quantitative evaluation of the performance of different PCM cells will be made by comparing the evolution of the S/L front (equivalently, the liquid volume) over time; more effective heat transfer will manifest as shorter melting or solidification times. The cells will be monitored along the Y and Z axes with a simple optical set-up, consisting of two cameras and a dedicated LED panel as a source of illumination. The principal camera will provide a lateral view of the cell and will be equipped with a telecentric lens to eliminate the parallax error characteristic of conventional lenses and more precisely measure the phase change process; this is achieved by having a constant non-angular field of view at any distance from the lens. The secondary camera will be used to check the two-dimensional character of the process and to provide an additional source of information.

The recorded images will be complemented by thermal measurements at key positions along the cell, which will allow us to distinguish different dynamical regimes according to the measured time dependence and, also, to have another (independent) diagnostic measurement of the PCM melting and solidification processes. For the cuboidal cell, the following temperature measurements are planned: three measurements points located near the left Peltier element and one near the right Peltier element in the XZ plane close to the lower boundary. The measurement locations near the left Peltier element include one in the XZ plane close to the bottom boundary of the cell and another in the XZ plane close to the upper PCM/air boundary, with the third placed at the same distance from the upper boundary but with an offset in Y. With the measurements close to the upper boundary, the presence and nature of oscillatory flows can be characterized [57]. The temperature readings near the bottom boundary will provide a secondary measurement of the phase change process. For the cylindrical cell, three temperature measurement points are planned near the left Peltier element and close to the free surface at different

Table 1
Experiment cell (EC) characteristics: EC number, type (Marangoni, Reference, Nano-enhanced Marangoni), geometry and content.

EC #	Type	Geometry	Content
1	Marangoni	Cuboidal	PCM + air/gas layer
2	Reference	Cuboidal	PCM
4	Marangoni	Cylindrical, $\Gamma = 2$	PCM + air/gas layer
4	Marangoni	Cylindrical, $\Gamma = 4$	PCM + air/gas layer
5	Nano-enhanced Marangoni	Cuboidal	PCM + metallic nanoparticles (FeCo) + air/gas layer
6	TBD	TBD	TBD

angles, and one measurement point near the right Peltier element at the center of the base. Again, the first three temperature readings will help distinguish different (azimuthal) oscillatory flow regimes [58] while that near the right Peltier element will record the arrival of the S/L front, i.e., the completion of melting.

As noted earlier, the MarPCM experiment is approved by ESA for execution on board the ISS. In particular, it is one of the experiments planned in the Microgravity Science Glovebox (MSG) [59], a sealed facility that provides an enclosed space for scientific investigations on the ISS. It can accommodate small and medium-sized experiments and provides the experiment with power, cooling resources, data acquisition, computer communications, vacuum, nitrogen, and other specialized tools.

The design and operational concept of the MarPCM experiment, described below, aim to minimize the use of ISS resources as much as possible while offering an appropriate level of flexibility to adjust scientific parameters during on-orbit operations.

The MarPCM design encompasses the following two modules (and elements):

1. Electronics and Computer Unit (ECU): This contains (i) the main experiment computer, (ii) hard drives for the operating system and the experimental data, and (iii) different electronic components. The ECU acts as a single electrical and data interface with MSG.
2. Experiment Cells and Diagnosis Unit (ECDU): These exchangeable units contain both the optical diagnostic systems and two experiment cells (ECs). They also include Peltier drivers, thermistor/thermocouple analog-to-digital converters, a USB hub for connecting the computer to these peripherals and electric conditioning devices. The ECDU will be placed in contact with the MSG base plate to evacuate heat.

A total of six experiment cells (three EDCUs) with varying cell geometry and PCMs will be processed on board, as summarized in Table 1. A series of runs will be performed with each cell using different thermal settings. Each of these individual runs is identified by the cell geometry (cuboidal, cylindrical), PCM material and applied temperatures. An initial estimate of the required operation time in the MSG is approximately 6–8 weeks.

The operational concept for the experiment anticipates the near real-time downlink of (i) scientific and housekeeping telemetry to monitor its evolution and status and (ii) selected high-resolution images to check and adjust, if appropriate, scientific parameters. Near real-time interaction with the experiment via telecommands is foreseen in order to allow ground operator tasks including the control of the experiment systems, interaction with Peltier elements, adjustment of the optical system settings, modification of the scientific scripts, and management of files in the experiment computer.

Although the quality of the microgravity present on the ISS is sufficient to obtain good scientific results, the precise microgravity level near the experiment's location (i.e., in the MSG working space) will be recorded during its execution and the impact of disturbances will be analyzed offline. Furthermore, crew contact with the MSG rack should be avoided. During the execution of the experiment, when part or all of the PCM is in the liquid state, a strong low-frequency acceleration (quasi-steady, with frequency < 0.01 Hz), such as may result from forceful crew contact with the rack, could potentially cause the liquid/gas interface to detach from the anchoring lines of the container, which would affect subsequent runs and possibly leave that experiment cell unusable for further science. In such a case, an assessment will be made as to whether the runs will be continued or not. Microgravity disturbances due to other ISS events will be evaluated as well.

As a result of the experiment execution, the following scientific data products are expected to be acquired: (i) high resolution images of the experiment cell, (ii) Peltier element temperatures and power consumption, (iii) temperature measurements inside the cells, (iv) temperature measurements near the cells and the MSG work volume and baseplate temperatures, and (v) microgravity measurements from a SAMS accelerometer [60].

All scientific data obtained during the experiment will be stored on a dedicated hard drive for thorough post-processing on ground. After the on-orbit operations, the experiment modules can be disposed of or stowed for future reuse. Depending on the operational concept for data downlink, two scenarios can be implemented for the hard drive containing the scientific data: (1) on-orbit disposal, if all scientific data is downlinked in near real-time, (2) return of the hard drive and delivery to the science team.

5. Expected results and hypotheses

As discussed earlier in Section 2, scientific expectations for the proposed experiment are drawn in large part from a preliminary parabolic flight experiment [26,40] and a series of numerical investigations using a two-dimensional model that was validated by comparison with those parabolic flight results [41].

Thermal Marangoni convection is capable of increasing the heat transfer rate by a significant factor, depending on the physical properties of the PCM [48], its geometry, and the applied temperatures [44,46] and there is every reason to think that this substantial improvement in PCM performance will be confirmed in microgravity. If the designs of the PCM devices also prove robust, then it may be hoped that the MarPCM results will lead to significant improvements in future designs for passive PCM applications in space missions.

In addition to the improvement of the average heat transfer rate, there are interesting dynamics related to oscillatory thermocapillary convection [39,45,51,52] that should be observed. This is due to the fact that the effective aspect ratio and Marangoni number vary as the volume of the liquid phase changes [39] and typically pass through values associated with oscillatory convection in comparable systems on ground and in liquid bridge experiments in microgravity. Simulations suggest that the oscillatory regime can further improve PCM performance for many aspect ratios by augmenting convective heat transfer [44].

The expectations for improvement in the heat transfer rate from convective motion are summarized in Fig. 6, where the ratio between melting times in (cuboidal) Reference and Marangoni cells of $\Gamma = 1.5$ (length $\times$ height $= 22.5 \times 15$ mm^2) is shown for increasing applied Marangoni number (i.e., applied ΔT). Two different scalings – associated with the presence of steady or oscillatory thermocapillary convection in the cell – are observed for increasing Ma; these flow regimes are distinguished by color: steady (black), OSW (blue), critical Ma for oscillatory flow (green). The proposed experiments, with corresponding data points filled in red, aim to explore these dynamics and

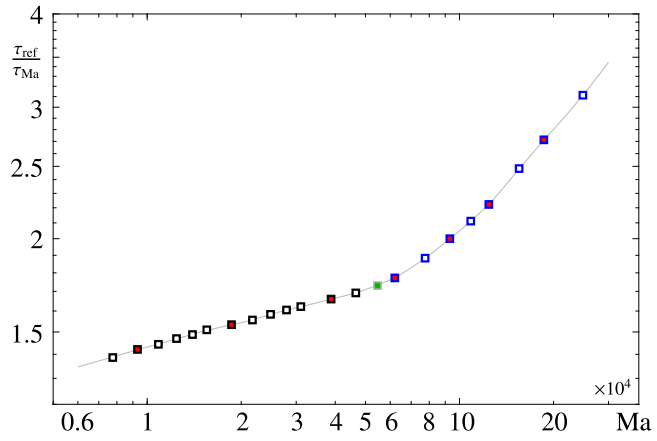

Fig. 6. Predicted ratios between melting times in Reference and Marangoni experiments in rectangular cells of $\Gamma = 1.5$ ($L \times H = 22.5 \times 15$ mm) as the applied Ma (ΔT) is varied. Two different scaling laws are observed, according to the presence of steady (black markers) or oscillatory convection (blue markers); the onset of oscillatory flow is marked in green. Filled markers denote some of the planned ISS experiments. (For interpretation of the references to color in this figure legend, the reader is referred to the web version of this article.)

confirm the predictions of the two-dimensional model. Note that the increase in heat transfer rate (decrease in melting time) for the Marangoni cell is on the order of a factor of 2, depending on temperature. Based on Ref. [46], we also expect a substantial heat transport enhancement in cylindrical geometry.

Moreover, due to the low thermal conductivity of the alkane family, the addition of metallic nanoparticles will be considered as a way to increase heat conduction. Previous studies have demonstrated that an appropriate choice of metallic nanoparticles can improve the performance of an NePCM device significantly [56]. In the MarPCM experiment, an improvement in the heat transfer rate of approximately 20% is expected from the nanoparticles [55].

Concerning the impact of g-jitter and vibrations on the experiment, it is not expected that residual ISS accelerations will affect the measurement of the heat transfer rate. However, high intensity perturbations may change the flow patterns established in the liquid phase [61] as well as the shape of the interface [48,62–65]. An analysis of this will require careful digital signal processing of accelerometric records coming from a location as close as possible to the experiment and capable of detecting the frequencies of interest [66].

6. Preliminary ground results

The MarPCM experiment is currently in the final design stage and manufacturing of the Engineering Model has begun. Prototypes of the cuboidal and cylindrical geometries have been built for engineering and scientific testing on ground; these are illustrated in Fig. 7 for (a) cuboidal and (b) cylindrical geometries. Note that the aspect ratio of the melting bridge ground prototype is substantially reduced compared to the cylindrical cell that will be used on the ISS. The reduction of Γ from 2 or 4 to 0.4 (length 4 mm and radius 10 mm) is necessary to allow a stable liquid bridge configuration when the PCM is completely melted on ground [67]. Aside from this change, the principal elements of the experiment described above can be identified in the photos.

The results of a melting experiment in a cuboidal Marangoni cell are shown in Fig. 8(a), where the evolution of the (cross-sectional) liquid fraction $\mathcal{L}$ (in %):

$$\mathcal{L} = \frac{1}{L \times H} \int (T \geq T_M) d\Omega, \tag{4}$$

is recorded for $\Delta T = 20$ K. The insets show the associated S/L front at selected times.

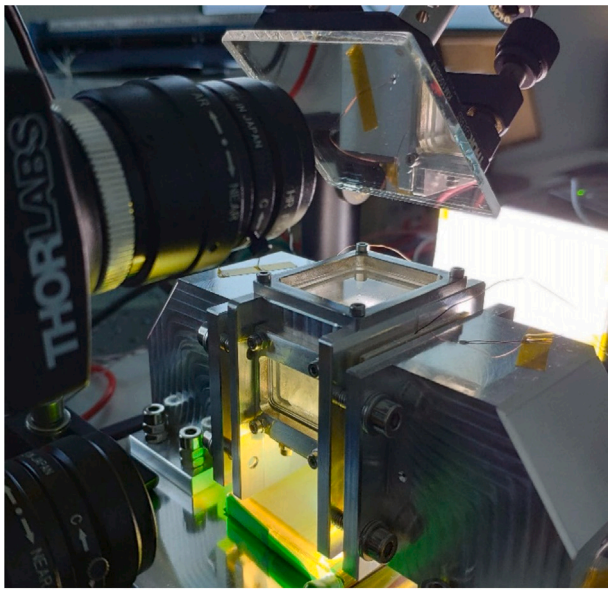

(a)

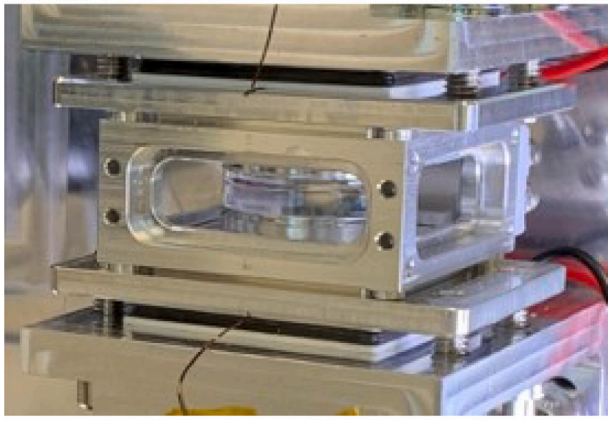

(b)

Fig. 7. Photos of ground prototypes for the MarPCM experiment for (a) cuboidal and (b) cylindrical (liquid bridge) geometries. Panel (a) also illustrates the optical set-up while (b) shows a close-up view.

As discussed above, the initial stage of the phase change process is dominated by conduction and characterized by horizontal progression of the S/L front. The exception to this arises near the liquid/air interface, where the thermocapillary effect locally accelerates heat transfer. As melting progresses and the S/L front separates sufficiently from the lateral wall, the effect of natural convection comes into play. The upper liquid layer, initially dominated by thermocapillary convection, widens and both types of convective flow contribute to the transport of heat [53]. The process continues until the entire PCM is liquefied and $\mathcal{L}$ reaches its limiting value of 100%; this point is marked by a vertical line in the figure and labeled as t_{melt}.

Various ground experiments with different ΔT have been performed to test the capabilities of the design and to compare with the predictions from numerical simulations with combined natural and thermocapillary convection [53]. These results, characterized by the melting time t_{melt}, are illustrated in Fig. 8(b) for applied temperature differences within the interval $\Delta T \in [5, 40]$ K. These are well fitted by the power law $t_{melt} \propto \Delta T^{-1.125}$.

During on-orbit operation, a preliminary evaluation is expected to be performed for each experiment run using the images downlinked in near real time. Similarly, the evolution of the phase change will be

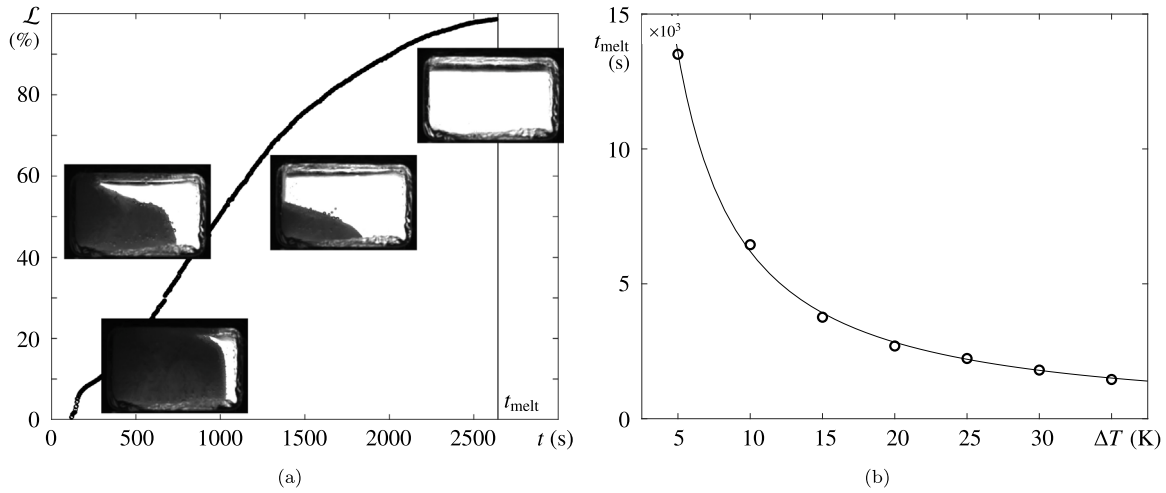

Fig. 8. Preliminary results from ground tests. (a) Evolution of the liquid area $\mathcal{L}$ in a cuboidal Marangoni cell with $\Delta T = 20$ K; melting finishes at $t = t_{melt}$. The insets show the solid and liquid phases at selected times. (b) Observed melting times t_{melt} when the thermal gradient is varied within the interval $\Delta T \in [5, 40]$ K.

evaluated via $\mathcal{L}$ for different runs and compared using the characteristic melting time t_{melt}. This type of preliminary evaluation will be useful for planning subsequent runs and for optimizing the use of ISS resources (power, thermal cooling, crew time, etc.).

Ground prototypes have also demonstrated the compatibility between the PCM and the experiment cells, which are made of aluminum, polymethyl methacrylate (PMMA) and nitrile rubber (NBR) O-rings. These same materials were used for manufacturing the cells of the TEPiM experiment [26], which are currently being utilized for ground tests with no observable degradation since their filling in 2016; hence, compatibility problems are not expected for the MarPCM experiment.

7. Conclusions

A range of present and future challenges in space exploration, like the development of Lunar habitats or the journey to Mars, call for improved thermal control systems. The "Effect of Marangoni Convection on Heat Transfer in Phase Change Materials" (MarPCM) experiment aims to contribute directly to current understanding of heat and mass transport in PCMs in reduced gravity and to the development of more efficient designs for heat management devices. The experiment is approved by ESA for implementation on board the ISS as one of the payloads to be executed inside the Microgravity Science Glovebox [59].

Specifically, MarPCM proposes to combine theoretical and experimental investigation in order to demonstrate the potential of thermocapillary (Marangoni) convection to expedite melting of organic PCMs and, thus, make more efficient use of their energy storage capacity. The scientific objectives can be summarized as follows:

1. Quantify the effect of thermal Marangoni convection on the heat transfer rate.
2. Compare the effectiveness of thermal Marangoni convection in cuboidal and cylindrical geometries.
3. Determine the dependence on temperature gradient of the thermocapillary contribution, including the effect of steady and oscillatory dynamics in the liquid.
4. Evaluate the robustness of the proposed design and any practical difficulties associated with PCM operation over a series of melting and freezing cycles.
5. Compare the heat transport efficiency of a pure PCM with that of a NePCM.
6. Investigate the effect of mechanical vibrations with and without thermal Marangoni convection.

The MarPCM experiment will drive controlled melting and solidification cycles through the application of fixed temperatures to opposite ends of a PCM sample, which will take either a cuboidal or a cylindrical shape. The phase change cycles will be observed by means of high-resolution optical cameras. The images they provide will be complemented by thermal measurements taken at key positions along the cells, and these thermal time series will allow for different dynamical regimes to be distinguished. A total of six experiment cells will be processed on board, with varying combinations of cell geometry and PCM. A series of runs will be performed with each cell using different thermal settings. The initial estimate of the required operation time for MarPCM is 6–8 weeks.

Scientific expectations for the proposed experiment are based on a preliminary parabolic flight experiment [26,40] and on a series of numerical investigations [41,44–46]. These indicate that thermal Marangoni convection can increase the heat transfer rate by a significant factor, on the order of 2 in this experiment. If that improvement is confirmed, and the PCM design proves robust, then the MarPCM results may lead to substantial improvements in future designs for passive PCM applications in space missions. Additionally, interesting and novel dynamics related to oscillatory thermocapillary convection may be observed [39,45,50,52,61].

The MarPCM experiment is in the final design stage for the manufacturing of the Engineering Model and prototypes of the cuboidal and cylindrical experiments have been built and tested in a series of ground experiments to evaluate the capabilities of the design and to compare with numerical simulations. These promising ground results were summarized in Section 6.

Declaration of competing interest

The authors declare that they have no known competing financial interests or personal relationships that could have appeared to influence the work reported in this paper.

Acknowledgments

The MarPCM project is supported by the Ministerio de Ciencia e Innovación, Spain under Project Nos. PID2020-115086GB-C31 (UPM), PID2020-115086GB-C32 (URV) and PID2020-115086GB-C33 (MU), and by the Spanish User Support and Operations Centre (E-USOC), Center for Computational Simulation, Spain (CCS). The MU team also acknowledges support from the Basque government, Spain under grants

No. IT1505-22 and No. 2022-CIEN-000052-01 (HOZTIKOR), associated with the Research Group Program and the Gipuzkoa Provincial Council, Spain, respectively. The URV contribution is further supported by the Universitat Rovira i Virgili, Spain under grant No. 2021PFRURV-74. Finally, the UPM team thanks the Escuela Técnica Superior de Ingeniería Aeronáutica y del Espacio and, in particular, the research group of Ciencias y Operaciones Aeroespaciales.

References

[1] N. Chaiyat, T. Kiatsiriroat, Energy reduction of building air-conditioner with phase change material in Thailand, Case Stud. Therm. Eng. 4 (2014) 175–186.
[2] K.O. Lee, M.A. Medina, Using phase change materials for residential air conditioning peak demand reduction and energy conservation in coastal and transitional climates in the state of California, Energy Build. 116 (2016) 69–77.
[3] R. Kandasamy, X.-Q. Wang, A.S. Mujumdar, Application of phase change materials in thermal management of electronics, Appl. Therm. Eng. 27 (17) (2007) 2822–2832.
[4] J. Hu, K.M. Babu, Fabric Testing: Testing Intelligent Textiles, Woodhead Publishing Series in Textiles, 2008.
[5] B. Pause, Smart Textile Coatings and Laminates: Phase Change Materials and their Applications in Coating and Laminates for Textiles, The Textile Institute Book Series, 2019.
[6] P.H. Biwole, P. Eclache, F. Kuznik, Phase-change materials to improve solar panel's performance, Energy Build. 62 (2013) 59–67.
[7] C.J. Ho, B.-T. Jou, C.-M. Lai, C.-Y. Huang, Performance assessment of a BIPV integrated with a layer of water-saturated MEPCM, Energy Build. 67 (2013) 322–333.
[8] A. Sharma, V.V. Tyagi, C.R. Chen, D. Buddhi, Review on thermal energy storage with phase change materials and applications, Renew. Sustain. Energy Rev. 13 (2009) 318–345.
[9] Y.B. Tao, Y.-L. He, A review of phase change material and performance enhancement method for latent heat storage system, Renew. Sustain. Energy Rev. 93 (2018) 245–259.
[10] G. Quinn, L. Hung, T. Ahlstrom, R. Sheth, Phase change material heat sink flight experiment results, in: 47th International Conference on Environmental Systems, 2017, pp. 1–18.
[11] H.M. Ettouney, I. Alatiqi, M. Al-Sahali, S.A. Al-Ali, Heat transfer enhancement by metal screens and metal spheres in phase change energy storage systems, Renew. Energy 29 (2004) 841–860.
[12] F. Agyenim, P. Eames, M. Smytha, A comparison of heat transfer enhancement in a medium temperature thermal energy storage heat exchanger using fins, Sol. Energy 83 (2004) 1509–1520.
[13] D. Fernandes, F. Pitié, G. Cáceres, J. Baeyens, Thermal energy storage: "How previous findings determine current research priorities", Energy 39 (2012) 1509–1520.
[14] A. Atal, Y. Wang, M. Harsha, S. Sengupta, Effect of porosity of conducting matrix on a phase change energy storage device, Int. J. Heat Mass Transfer 93 (2016) 9–16.
[15] S.F. Hosseinizadeh, A.A. Rabienataj Darzi, F.L. Tan, Numerical investigations of unconstrained melting of nano-enhanced phase change material (NEPCM) inside a spherical container, Int. J. Therm. Sci. 51 (2012) 77–83.
[16] N.S. Dhaidan, J.M. Khodadadi, T.A. Al-Hattab, S.M. Al-Mashat, Experimental and numerical investigation of melting of NePCM inside an annular container under a constant heat flux including the effect of eccentricity, Int. J. Heat Mass Transfer 67 (2013) 455–468.
[17] C. Gau, R. Viskanta, Melting and solidification of a pure metal on a vertical wall, J. Heat Transfer 108 (1986) 174–181.
[18] S.K. Roy, S. Sengupta, Gravity-assisted melting in a spherical enclosure: Effects of natural convection, Int. J. Heat Mass Transfer 33 (1990) 1135–1147.
[19] Y. Wang, A. Amiri, K. Vafai, An experimental investigation of the melting process in a rectangular enclosure, Int. J. Heat Mass Transfer 42 (1999) 3659–3672.
[20] J.M. Khodadadi, Y. Zhang, Effects of buoyancy-driven convection on melting within spherical containers, Int. J. Heat Mass Transfer 44 (2001) 1605–1618.
[21] H. Shokouhmand, B. Kamkari, Experimental investigation on melting heat transfer characteristics of lauric acid in a rectangular thermal storage unit, Exp. Therm. Fluid Sci. 50 (2013) 201–212.
[22] N.S. Dhaidan, J.M. Khodadadi, Melting and convection of phase change materials in different shape containers: A review, Renew. Sustain. Energy Rev. 43 (2015) 449–477.
[23] R. Creel, Apollo rover lessons learned: Applying thermal control experiences on apollo lunar rover project to rovers for future space exploration, 2007.
[24] www.esa.int/Education/Teach_with_the_Moon/ESA_Euronews_Moon_Village. (Accessed December 2022).
[25] A. Borshchak Kachalov, P. Salgado Sanchez, U. Martinez, J.M. Ezquerro, Preliminary design of a space habitat thermally controlled using phase change materials, Thermo 3 (2023) 232–247.
[26] J.M. Ezquerro, A. Bello, P. Salgado Sánchez, A. Laverón-Simavilla, V. Lapuerta, The thermocapillary effects in phase change materials in microgravity experiment: Design, preparation and execution of a parabolic flight experiment, Acta Astronaut. 162 (2019) 185–196.
[27] S. Madruga, C. Mendoza, Enhancement of heat transfer rate on phase change materials with thermocapillary flows, Eur. Phys. J. Spec. Top. 226 (2017) 1169–1176.
[28] S. Madruga, C. Mendoza, Heat transfer performance and melting dynamic of a phase change material subjected to thermocapillary effects, Int. J. Heat Mass Transfer 109 (2017) 501–510.
[29] D. Schwabe, A. Scharmann, Some evidence for the existence and magnitude of a critical Marangoni number for the onset of oscillatory flow in crystal growth melts, J. Cryst. Growth 46 (1979) 125–131.
[30] F. Preisser, D. Schwabe, A. Scharmann, Steady and oscillatory thermocapillary convection in liquid columns with free cylindrical surface, J. Fluid Mech. 126 (1983) 545–567.
[31] M. Lappa, R. Savino, 3D analysis of crystal/melt interface shape and Marangoni flow instability in solidifying liquid bridges, J. Comput. Phys. 180 (2002) 751–774.
[32] M. Lappa, On the formation and propagation of hydrothermal waves in liquid layers with phase change, Comput. & Fluids 172 (2018) 741–760.
[33] F.J. Higuera, Liquid-fuel thermocapillary flow induced by a spreading flame, J. Fluid Mech. 473 (2002) 349–377.
[34] W.A. Sirignano, I. Glassman, Flame spreading above liquid fuels: Surface tension driven flows, Combust. Sci. Technol. 1 (1970) 307–312.
[35] M. Lappa, On the propagation of hydrothermal waves in a fluid layer with two-way coupled dispersed solid particles, Fluids 7 (2022) 215.
[36] A.K. Sen, S.H. Davis, Steady thermocapillary flows in two-dimensional slots, J. Fluid Mech. 121 (1982) 163–186.
[37] L.J. Peltier, S. Biringen, Time-dependent thermocapillary convection in a rectangular cavity: Numerical results for a moderate Prandtl number fluid, J. Fluid Mech. 257 (1993) 339–357.
[38] H.C. Kuhlmann, S. Albensoeder, Three-dimensional flow instabilities in a thermocapillary-driven cavity, Phys. Rev. E 77 (2008) 036303.
[39] P. Salgado Sanchez, J. Porter, J.M. Ezquerro, I. Tinao, A. Laveron-Simavilla, Pattern selection for thermocapillary flow in rectangular containers in microgravity, Phys. Rev. Fluids 7 (2022) 053502.
[40] J.M. Ezquerro, P. Salgado Sánchez, A. Bello, J. Rodríguez, V. Lapuerta, A. Laverón-Simavilla, Experimental evidence of thermocapillarity in phase change materials in microgravity: Measuring the effect of Marangoni convection in solid/liquid phase transitions, Int. Commun. Heat Mass Transfer 113 (2020) 104529.
[41] P. Salgado Sánchez, J.M. Ezquerro, J. Porter, J. Fernández, I. Tinao, Effect of thermocapillary convection on the melting of phase change materials in microgravity: Experiments and simulations, Int. J. Heat Mass Transfer 154 (2020) 119717.
[42] V. Pletser, S. Rouquette, U. Friedrich, J.F. Clervoy, T. Gharib, F. Gai, C. Mora, The first European parabolic flight campaign with the airbus A310 ZERO-G, Microgravity Sci. Technol. 28 (2016) 587–601.
[43] E. Chen, F. Xu, Transient Marangoni convection induced by an isothermal sidewall of a rectangular liquid pool, J. Fluid Mech. 928 (2021) A6.
[44] P. Salgado Sanchez, J.M. Ezquerro, J. Fernandez, J. Rodriguez, Thermocapillary effects during the melting of phase change materials in microgravity: Heat transport enhancement, Int. J. Heat Mass Transfer 163 (2020) 120478.
[45] P. Salgado Sanchez, J.M. Ezquerro, J. Fernandez, J. Rodriguez, Thermocapillary effects during the melting of phase change materials in microgravity: Steady and oscillatory flow regimes, J. Fluid Mech. 908 (2021) A20.
[46] R. Varas, P. Salgado Sánchez, J. Porter, J.M. Ezquerro, V. Lapuerta, Thermocapillary effects during the melting in microgravity of phase change materials with a liquid bridge geometry, Int. J. Heat Mass Transfer 178 (2021) 121586.
[47] V. Shevtsova, D.E. Melnikov, A. Nepomnyashchy, New flow regimes generated by mode coupling in buoyant-thermocapillary convection, Phys. Rev. Lett. 102 (2009) 134503.
[48] N. Garcia-Acosta, P. Salgado Sanchez, J. Jimenez, U. Martinez, J.M. Ezquerro, Thermocapillary–enhanced melting of different phase–change materials in microgravity, Microgravity Sci. Technol. 34 (2022) 92.
[49] A. Borshchak Kachalov, P. Salgado Sánchez, U. Martínez, J. Fernández, J.M. Ezquerro, Optimization of thermocapillary-driven melting in trapezoidal and triangular geometry in microgravity, Int. J. Heat Mass Transfer 185 (2022) 122427.
[50] N. Martínez, P. Salgado Sanchez, J. Porter, J.M. Ezquerro, Effect of surface heat exchange on phase change materials melting with thermocapillary flow in microgravity, Phys. Fluids 33 (2021) 083611.
[51] B. Seta, D. Dubert, J. Massons, J. Gavalda, M. Mounir Bou-Ali, X. Ruiz, Effect of Marangoni induced instabilities on a melting bridge under microgravity conditions, Int. J. Heat Mass Transfer 179 (2021) 121665.
[52] B. Seta, D. Dubert, M. Prats, J.G.J. Massons, M.M. Bou-Ali, X. Ruiz, V. Shevtsova, Transitions between nonlinear regimes in melting and liquid bridges in microgravity, Int. J. Heat Mass Transfer 193 (2022) 122984.

[53] A. Borshchak Kachalov, P. Salgado Sánchez, J. Porter, J.M. Ezquerro, The combined effect of natural and thermocapillary convection on the melting of phase change materials in rectangular containers, Int. J. Heat Mass Transfer 168 (2021) 120864.
[54] R. Varas, U. Martinez, K. Olfe, P. Salgado Sanchez, J. Porter, J.M. Ezquerro, Effects of thermocapillary and natural convection during the melting of phase change materials with a liquid bridge geometry, Microgravity Sci. Technol. 35 (2023) 17.
[55] P. Salgado Sanchez, J.M. Ezquerro, J. Porter, J. Fernandez, J. Rodriguez, I. Tinao, V. Lapuerta, A. Laveron-Simavilla, X. Ruiz, F. Gavalda, M.M. Mounir Bou-Ali, J. Ortiz, The effect of thermocapillary convection on PCM melting in microgravity: Results and expectations, in: Proceeding of the 72th International Astronautical Conference, IAC, 2020.
[56] S. Madruga, C. Mendoza, Heat transfer performance and thermal energy storage in nano-enhanced phase change materials driven by thermocapillarity, Int. Commun. Heat Mass Transfer 129 (2021) 105672.
[57] B. Seta, P. Salgado Sánchez, J. Massons, J. Gavalda, J. Porter, M.M. Bou-Ali, X. Ruiz, V. Shevtsova, Three-dimensional effects during the melting of phase-change materials with thermocapillary flow in microgravity, in: 27th European Low Gravity Research Association Biennial Symposium and General Assembly, 2022, pp. 1–2.
[58] Y. Gaponenko, V. Yasnou, A. Mialdun, A. Nepomnyashchy, V. Shevtsova, Effect of the supporting disks shape on nonlinear flow dynamics in a liquid bridge, Phys. Fluids 33 (2021) 042111.
[59] www.nasa.gov/centers/marshall/history/msg.html. (Accessed December 2022).
[60] https://gipoc.grc.nasa.gov/wp/pims/home/. (Accessed December 2022).
[61] B. Seta, D. Dubert, J. Massons, P. Salgado Sanchez, J. Porter, J. Gavalda, M.M. Bou-Ali, X. Ruiz, On the impact of body forces in low Prandtl number liquid bridges, in: Advanced Technologies, Systems, and Applications V, in: Lecture Notes in Networks and Systems, vol. 142, 2021, pp. 217–227.
[62] C. Ferrera, M.A. Herrada, J.M. Montanero, Analysis of a resonance liquid bridge oscillation on board of the International Space Station, Eur. J. Mech. B/Fluids 57 (2016) 15–21.
[63] D. Gligor, P. Salgado Sánchez, J. Porter, I. Tinao, Thermocapillary-driven dynamics of a free surface in microgravity: Response to steady and oscillatory thermal excitation, Phys. Fluids 34 (4) (2022) 042116.
[64] D. Gligor, P. Salgado Sánchez, J. Porter, J.M. Ezquerro Navarro, Thermocapillary-driven dynamics of a free surface in microgravity: Control of sloshing, Phys. Fluids 34 (2022) 072109.
[65] P. Salgado Sanchez, U. Martinez, D. Gligor, I. Torres, J. Plaza, J.M. Ezquerro, The ‘‘thermocapillary-based control of a free surface in microgravity" experiment, Acta Astronaut. 205 (2023) 57–67.
[66] D. Dubert, J. Olle, R. Jurado, J. Gavalda, A. Laveron-Simavilla, X. Ruiz, V. Shevtsova, Characterization of the accelerometric environment of DCMIX2/3 experiments, Microgravity Sci. Technol. 30 (2018) 683—697.
[67] L.A. Slobozhanin, J.M. Perales, Stability of liquid bridges between equal disks in an axial gravity field, Phys. Fluids 5 (6) (1993) 1305–1314.